Journal of the Oceanographical Society of Japan
Vol. 39, pp. 43 to 52, 1983

Backscatter of Microwaves from the Sea Surface and the Modulation of Spectra of Short Gravity Waves*

Noriyuki IWATA**

Abstract: Backscatter cross-sections of microwaves from the sea surface are calculated by using the facet model and are compared with JONSWAP '75 experimental results. The principal features obtained are: (1) asymmetry of backscatter cross-sections between upwind and downwind directions is attributable to the modulation of the short gravity-capillary wave spectrum by a larger wave, and the non-Gaussian wave slope distribution has a tendency to cancel this effect, (2) angular spreading of the energy spectrum in the higher frequency range should have a narrower band than a simple cosine distribution, (3) the facet model itself should begin to break down at a larger incident angle than previously supposed.

1. Introduction

Significant advances have been made in the last three decades towards understanding the basic phenomena involved in the scatter of microwaves from the sea surface (RICE, 1951; WRIGHT, 1966; BARRICK and PEAKE, 1967 (Chap. II); BASS *et al.*, 1968a, b). From these investigations it has been established that the most important mechanism contributing to the scattering of electromagnetic waves from the roughned water surface is the *Bragg* or *resonant* mechanism except for specular scatter, which predominates when the incident angle remains within near nadir angles.

In order to apply these results to the real ocean, we must take into account the role played by larger ocean waves which not only tilt the roughned surface but also modify the spectrum of short waves on that surface (VALENZUELLA, 1968; FUNG and CHANG, 1969). This is the so-called composite rough surface model and this general model may be further subdivided into two cases: (1) The large undulations are larger in dimension than that of the illuminated area so that within the beam of illumination the picture is a tilted perturbed plane. (2) The large undulations are such a size that at least several undulations can be found within the beam. The former is essentially the small perturbation model. The latter is much more complicated and has been approached in most cases under a non-coherent assumption, *i.e.*, the contributions from the small irregularities may be computed by summing powers from the large undulations so that it is often called the wave-facet model. The total contribution from the composite surface is then taken to be that from the large undulations plus that from the small irregularities averaged over the large undulations. Although it is desirable to deal with a coherent model taking the slope distributions into consideration, it is not practical because analysis using the coherent model becomes very complicated (CHANG and FUNG, 1973; Appendix IV).

In this paper the non-coherent, wave-facet model is used and in order to compare our results with CHANG and FUNG (1977) as well as WENTZ (1978) we have imposed the following restrictions on the model:

(1) the frequency of the emitted microwave is 13.9 GHz (CHANG and FUNG, WENTZ),
(2) the dielectric constant of seawater is assumed to be 40.1–i39.3 (WENTZ),
(3) the power spectrum of the small gravity-capillary waves is taken from PIERSON (1976) (CHANG and FUNG),
(4) the probability distribution function of the ocean wave slope is taken from COX and MUNK (1954) (CHANG and FUNG),
(5) hydrodynamic modulation of the short

* Received Nov. 14, 1981, revised Nov. 1 and accepted Dec. 8, 1982.
** Institute of Coastal Oceanology, National Research Center for Disaster Prevention, Science and Technology Agency, Nijigahama, Hiratsuka, Kanagawa 254, Japan

gravity-capillary waves due to undulation is assumed to be proportional to the slope of the undulation (WENTZ),

(6) instead of numerical integration of Eq. (8) the integrand is expanded in power series and then integrated (WENTZ).

CHANG and FUNG (1977) allowed for the kinematical tilting effect but did not take into account the hydrodynamical modulation of short gravitty-capillary waves and as a result they attributed the asymmetry of backscatter between upwind and downwind directions to the non-Gaussian wave slope distribution. In contrast WENTZ (1978) ignored this non-Gaussian distribution and considered the hydrodynamical modulation to be the principal factor behind this asymmetry.

From the following numerical analyses it is clearly shown that the asymmetry of the backscatter is due to the hydrodynamical nonlinear interaction between an undulation and superimposed short waves and that the non-Gaussian slope distribution has a tendency to cancel the hydrodynamical effect.

The second result obtained is that the angular spreading of the energy spectrum in the higher frequency range should have a narrower band than that used in this paper.

The third and last conclusion to be drawn is that the wave-facet model itself should begin to break down at a somewhat larger incident angle than Wentz's estimated value.

2. Backscatter cross-section

It is widely accepted that except for angles near normal or near grazing incidence the general features of microwaves reflected from the sea surface can be explained well by the lowest-order Bragg scattering theory, *i.e.*, according to the electromagnetic scattering perturbation theory, the backscatter cross-section per unit area of the surface is given by

$$\sigma^0(\boldsymbol{k}^i)=T(\theta)[F(2\underline{\boldsymbol{k}}^i)+F(-2\underline{\boldsymbol{k}}^i)] \quad (1)$$

where $\boldsymbol{k}^i=(\underline{\boldsymbol{k}}^i, \boldsymbol{k}_3{}^i)$ denotes wave number of incident microwave and $T(\theta)$ is a function of polarization and incident angle θ,

$$T(\theta)=4\pi k^4\cos^4\theta|\alpha_{pp}|^2 \quad (2)$$

where for horizontal and vertical polarization $p=H$ and $p=V$ respectively, so that

$$\alpha_{HH}=\frac{\varepsilon-1}{[\cos\theta+\sqrt{\varepsilon-\sin^2\theta}]^2} \quad (3)$$

$$\alpha_{VV}=\frac{(\varepsilon-1)[\varepsilon+(\varepsilon-1)\sin^2\theta]}{[\varepsilon\cos\theta+\sqrt{\varepsilon-\sin^2\theta}]^2} \quad (4)$$

where $k=|\boldsymbol{k}^i|$, ε is a complex dielectric constant of the sea water and $F(\boldsymbol{k}_B)$ shows $\boldsymbol{k}_B$ component of a two-dimensional ocean surface wave spectrum.

For electromagnetic waves, the ocean surface appears frozen, so that not only $F(\boldsymbol{k}_B)$ but also $F(-\boldsymbol{k}_B)$ contributes to the backscatter cross-section, independent of the direction of propagation of the ocean wave. For X-band electromagnetic waves, the following form of a directional spectrum of the sea surface roughness for the so-called MITSUYASU and HONDA (1974) range is taken (PIERSON 1976: pp. 304-308)

$$F(\boldsymbol{k}_B)+F(-\boldsymbol{k}_B)=S(\boldsymbol{k}_B)=\frac{S_4(k_B)}{2\pi}\left[1+2\frac{1-R}{1+R}\cos 2\phi\right], \quad k_*>k_B>0.942 \quad (5)$$

$$S_4(k_B)=0.875(2\pi)^{p-1}\times\frac{g\left\{1+3\left(\frac{k_B}{k_m}\right)^2\right\}}{k_B\left[gk_B\left\{1+\left(\frac{k_B}{k_m}\right)^2\right\}\right]^{\frac{p+1}{2}}} \quad (6)$$

where

$$k_B=2k\sin\theta,\quad k_m=\left(\frac{g\rho}{\tau}\right)^{1/2},\quad R=\frac{\langle n_2{}^2\rangle}{\langle n_1{}^2\rangle}$$

$$p=5.0-\log_{10}u_*,\quad U=\frac{u_*}{0.4}\ln\frac{1250}{z_0}$$

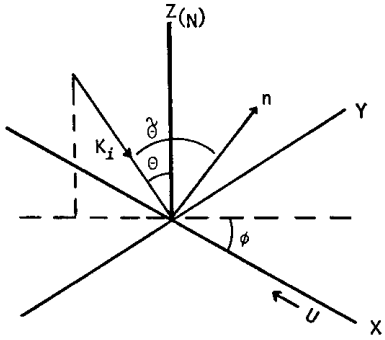

Fig. 1. Diagram of the coordinate system.

$$z_0=\frac{0.684}{u_*}+4.28\times10^{-5}\,u_*{}^2-4.43\times10^{-2},$$

where ϕ is azimuth angle refered to the upwind direction as shown in Fig. 1 $\langle n_1{}^2\rangle$, $\langle n_2{}^2\rangle$ represent slope variance in the upwind and crosswind directions respectively. The notation τ is the surface tension, u_* is the friction velocity of the wind and k_ν is the wavenumber at the intersection point of the above spectrum $S_4(k_B)$ and the following spectrum for the COX viscous cutoff range (PIERSON and STACY 1973; pp. 48-53)

$$S_5(g_B)\sim\frac{u^3{}_*}{g\nu}\frac{k^6{}_m}{k_B{}^{10}} \qquad (7)$$

For X- or Ku-band of radar frequency we find that for almost all significant cases $k_\nu>k_B$ so that we can ignore all the other parts of the ocean wave spectrum except $S_4(k_B)$.

To include the tilting effect of an undulation it is necessary to take into account the variation of the incident angle as wel as of polarization relative to the local scattering plane (electromagnetic modulation) and also the modulation of the short wave spectrum due to undulation (hydrodynamic modulation).

If $p(n_1, n_2)$ represents the probability density distribution of large scale wave slope $n_\alpha=\partial\zeta_s/\partial x_\alpha$, the scattering cross-section in the wave-facet model is given by,

$$\sigma^0=\int\tilde{\boldsymbol{T}}(\tilde\theta)[\tilde{\boldsymbol{F}}(2\underline{\tilde{\boldsymbol{k}}}_i)+\tilde{\boldsymbol{F}}(-2\underline{\tilde{\boldsymbol{k}}}_i)]p(n_1,n_2)dn_1dn_2 \qquad (8)$$

where the tilde denotes quantities defined with respect to the local large-scale wave. The function $\tilde{\boldsymbol{T}}(\tilde\theta)$ shows modification $T(\theta)$ through $\theta\to\tilde\theta$ and $\underline{\boldsymbol{k}}_i\to\underline{\tilde{\boldsymbol{k}}}_i$ in addition to a rotation of the polarization axes (see Fig. 1).

If we take coordinate axis on the undisturbed sea level with the z axis vertically upwards and the x-axis along the upwind direction as shown in Fig. 1, we have (WENTZ 1978; pp. 3-6)

$$\tilde{\boldsymbol{T}}(\tilde\theta)=4\pi k^4\cos^4\tilde\theta\,(\boldsymbol{n}\cdot\boldsymbol{N})^{-1}\times S_{is}(\boldsymbol{k}_i,\boldsymbol{E}_i:\,-\boldsymbol{k}_i,E_s;\,\boldsymbol{n}) \qquad (9)$$

$$S_{is}(\boldsymbol{k}_i,\boldsymbol{E}_i;\,-\boldsymbol{k}_i,\boldsymbol{E}_s;\,\boldsymbol{n})=|(\boldsymbol{E}_i\cdot\boldsymbol{e}_V)(\boldsymbol{E}_s{}^*\cdot\boldsymbol{e}_V)\tilde\alpha_{VV}+(\boldsymbol{E}_i\cdot\boldsymbol{e}_h)(\boldsymbol{E}_s{}^*\cdot\boldsymbol{e}_h)\tilde\alpha_{HH}|^2 \qquad (10)$$

where $\boldsymbol{k}_i$ is an incident propagation unit-vector, and $\boldsymbol{E}_i$ and $\boldsymbol{E}_s$ are the incident and scattered polarization unit-vectors,

$$\left.\begin{aligned}\boldsymbol{E}_H&=-\frac{\boldsymbol{k}_i\times\boldsymbol{N}}{|\boldsymbol{k}_i\times\boldsymbol{N}|},\quad \boldsymbol{e}_h=-\frac{\boldsymbol{k}_i\times\boldsymbol{n}}{|\boldsymbol{k}_i\times\boldsymbol{n}|}\\ \boldsymbol{E}_V&=\boldsymbol{k}_i\times\boldsymbol{E}_H\quad,\quad \boldsymbol{e}_V=\boldsymbol{k}_i\times\boldsymbol{e}_h\end{aligned}\right\} \qquad (11)$$

and $\tilde\alpha_{pp}$ is given by (3) and (4) when θ is replaced by $\tilde\theta$, *i.e.*, the local incident angle refered to the large-scale wave surface. The symbol $\boldsymbol{N}$ denotes a unit vector normal to the mean sea level, whereas $\boldsymbol{n}$ is unit vector normal to the local large-scale wave surface. From the above definition it turns out after simple algebra that

$$S_{HH}(\boldsymbol{k}_i,\boldsymbol{E}_H;-\boldsymbol{k}_i,\boldsymbol{E}_H;\,\boldsymbol{n})=|(\boldsymbol{E}_V\cdot\boldsymbol{e}_h)|^2\tilde\alpha_{VV}+|\boldsymbol{E}_H\cdot\boldsymbol{e}_h|^2\tilde\alpha_{HH}|^2 \qquad (12)$$

$$S_{VV}(\boldsymbol{k}_i,\boldsymbol{E}_V;\,-\boldsymbol{k}_i,\boldsymbol{E}_V;\,\boldsymbol{n})=|(\boldsymbol{E}_H\cdot\boldsymbol{e}_h)|^2\tilde\alpha_{VV}+|\boldsymbol{E}_V\cdot\boldsymbol{e}_h|^2\tilde\alpha_{HH}|^2 \qquad (13)$$

When we refer to the coordinate axis as shown in Fig. 1, we get

$$\boldsymbol{n}=\frac{1}{\sqrt{1+n_1{}^2+n_2{}^2}}(-n_1\boldsymbol{i}-n_2\boldsymbol{j}+\boldsymbol{N}) \qquad (14)$$

$$\boldsymbol{k}_i=\sin\theta\cos\phi\boldsymbol{i}+\sin\theta\sin\phi\boldsymbol{j}-\cos\theta\boldsymbol{N} \qquad (15)$$

By substituting $\boldsymbol{n}$ and $\boldsymbol{k}_i$ in (11), we obtain,

$$\boldsymbol{E}_V\cdot\boldsymbol{e}_h=\frac{1}{D}[n_2\cos\phi-n_1\sin\phi] \qquad (16)$$

$$\boldsymbol{E}_H\cdot\boldsymbol{e}_h=\frac{1}{D}[\sin\theta-\cos\theta(n_2\sin\phi+n_1\cos\phi)] \qquad (17)$$

$$D^2=\sin^2\theta+\cos^2\theta\cdot(n_1{}^2+n_2{}^2)-\sin2\theta\cdot(n_1\cos\phi+n_2\sin\phi)+\sin^2\theta\cdot(n_1\sin\phi-n_2\cos\phi)^2 \qquad (18)$$

and

$$\cos\tilde\theta=\frac{1}{\sqrt{1+n_1{}^2+n_2{}^2}}\times[(n_1\cos\phi+n_2\sin\phi)\sin\theta+\cos\theta] \qquad (19)$$

$$\sin\tilde\theta=\frac{D}{\sqrt{1+n_1{}^2+n_2{}^2}} \qquad (20)$$

We can see that $\tilde{\boldsymbol{T}}(\tilde\theta)$ is a function of incident angle θ, azimuth angle ϕ and the slope of the large-scale wave n_1, n_2.

The probability density function of a large-scale surface wave slope $p(n_1n_2)$ is assumed to be given by (COX and MUNK, 1954),

$$p(n_1, n_2)=\frac{1+Q(\mu,\nu)}{2\pi\sqrt{\langle n_1^2\rangle}\sqrt{\langle n_2^2\rangle}}e^{-1/2(\mu^2+\nu^2)} \quad (21)$$

$$\mu=\frac{n_1}{\sqrt{\langle n_1^2\rangle}},\quad \nu=\frac{n_2}{\sqrt{\langle n_2^2\rangle}} \quad (22)$$

$$\begin{aligned}Q(\mu,\nu)=&c_1\mu(\nu^2-1)+c_2\mu(\mu^2-3)\\&+c_3(\nu^4-6\nu^2+3)+c_4(\nu^2-1)(\mu^2-1)\\&+c_5(\mu^4-6\mu^2+3)\end{aligned} \quad (23)$$

where

$$c_1=-\frac{1}{2}(0.01-0.0086U),$$

$$c_2=-\frac{1}{6}(0.04-0.033U)$$

$$c_3=\frac{0.1}{6},\ c_4=0.03,\ c_5=\frac{0.23}{24}$$

$$\langle n_1^2\rangle=3.16\times10^{-3}U,$$

$$\langle n_2^2\rangle=0.003+1.92\times10^{-3}U$$

where $\langle n_1^2\rangle$ is the slope variance in the upwind direction, and $\langle n_2^2\rangle$ is in the crosswind direction. It must be noticed, however, that the wind velocity on the right-hand side is in meters per sec and at an altitude of 12.5 m above the sea level, whereas in (6) it is represented in c.g.s. units.

The backscatter cross-section in the wave-facet model can be rewritten as,

$$\sigma^0=\frac{1}{2\pi}\int\tilde{T}^*(\mu,\nu,\theta,\phi)\tilde{S}(\tilde{k}_B)e^{-1/2(\mu^2+\nu^2)}d\mu d\nu \quad (24)$$

$$\tilde{T}^*(\mu,\nu,\theta,\phi)=\tilde{T}(\tilde{\theta})[1+Q(\mu,\nu)],$$

$$\tilde{S}(\tilde{k}_B)=\tilde{F}(\tilde{k}_B)+\tilde{F}(-\tilde{k}_B) \quad (25)$$

Now we assume that the hydrodynamical modulation ΔS is small and can be represented as,

$$\tilde{S}(\tilde{k}_B)=S(\tilde{k}_B)+\Delta S(\tilde{k}_B) \quad (26)$$

where

$$\tilde{k}_B=2\tilde{k}_i$$

When we expand $S(\tilde{k}_B)$ and $\tilde{T}^*(\mu,\nu,\theta,\phi)$ in power series of n_α, $(\alpha=1,2)$ and substitute them in (24), we get the leading terms (HASSELMANN 1971),

$$\begin{aligned}\sigma^0=&\tilde{\sigma}_0+\frac{1}{2}\left(\frac{\partial^2\tilde{\sigma}}{\partial n_\alpha\partial n_\beta}\right)_0\langle n_\alpha n_\beta\rangle\\&+\left[\frac{\partial\tilde{T}^*(\mu,\nu,\theta,\phi)}{\partial n_\alpha}\right]_0\langle\Delta S(\tilde{k}_B)n_\alpha\rangle+\cdots\end{aligned} \quad (27)$$

where the subscript zero refers to values at $n_\alpha=0$ and

$$\tilde{\sigma}(\mu,\nu)=\tilde{T}^*(\mu,\nu,\theta,\phi)S(\tilde{k}_B) \quad (28)$$

$$\langle n_\alpha n_\beta\rangle=\frac{1}{2\pi}\int_{-\infty}^{\infty}n_\alpha n_\beta e^{-1/2(\mu^2+\nu^2)}d\mu d\nu \quad (29)$$

where $\tilde{\sigma}$ denotes electrodynamic tilting modulation of the backscatter cross-section. When we replace the differential dn_α by the finite difference $\Delta n_\alpha=\sqrt{\langle n_\alpha^2\rangle}$ we get $\mu=1$ for $\alpha=1$, $\nu=1$ fo $\alpha=2$ and the second term of the right-hand side of (27) turns out to be (WENTZ, 1978: eq. (25))

$$\begin{aligned}\frac{1}{2}\left(\frac{\partial^2\tilde{\sigma}}{\partial n_1^2}\right)_0+\frac{1}{2}\left(\frac{\partial^2\tilde{\sigma}}{\partial n_2^2}\right)_0=&\frac{1}{2}[\tilde{\sigma}(1,0)+\tilde{\sigma}(-1,0)\\&+\tilde{\sigma}(0,1)+\tilde{\sigma}(0,-1)]-2\tilde{\sigma}(0,0)\end{aligned} \quad (30)$$

where $\tilde{\sigma}(1,0)$ means $\tilde{\sigma}(\mu,\nu)|_{\mu=1,\ \nu=0}$.

For the third term representing hydrodynamical modulation, we can put (WENTZ, 1978: eq. (27))

$$\Delta S(\tilde{k}_B)=B\mu S(k_B) \quad (31)$$

We assume that the wind blows toward the negative x-direction so that a positive B means that the intensity of the spectrum on the downwind side of a large-scale wave is higher than that on the upwind side.

For the third term of the right-hand side of (27) we similarly get

$$\begin{aligned}\left(\frac{\partial\tilde{T}^*}{\partial n_\alpha}\right)_0\langle\Delta S(\tilde{k}_B)n_\alpha\rangle=&\frac{B}{2}S(k_B)\\&\times[\tilde{T}^*(1,0;\ \theta,\phi)-\tilde{T}^*(-1,0;\ \theta,\phi)]\end{aligned} \quad (32)$$

The final form of the backscatter cross-section is given by

$$\begin{aligned}\sigma^0=&\frac{S(k_B)}{2}[-2\tilde{T}(0,0;\ \theta,\phi)\{1+Q(0,0)\}\\&+\tilde{T}(-1,0;\ \theta,\phi)\{1+Q(-1,0)\}\\&+\tilde{T}(1,0;\ \theta,\phi)\{1+Q(1,0)\}\\&+\tilde{T}(0,-1;\ \theta,\phi)\{1+Q(0,-1)\}\\&+\tilde{T}(0,1;\ \theta,\phi)\{1+Q(0,1)\}\\&+B\{\tilde{T}(1,0;\ \theta,\phi)(1+Q(1,0))\\&-\tilde{T}(-1,0;\ \theta,\phi)(1+Q(-1,0))\}]\end{aligned} \quad (33)$$

where

$$\tilde{T}(\mu,\nu;\ \theta,\phi)$$
$$=4\pi k^4\frac{[n_1\cos\phi+n_2\sin\phi)\sin\theta+\cos\theta]^4}{[1+n_1^2+n_2^2]^{3/2}}$$
$$\times\frac{1}{D^4}\left|\{\sin\theta-\cos\theta(n_2\sin\phi+n_1\cos\phi)\}^2\begin{Bmatrix}\tilde{\alpha}_{VV}\\ \tilde{\alpha}_{HH}\end{Bmatrix}\right.$$
$$\left.+(n_2\cos\phi-n_1\sin\phi)^2\begin{Bmatrix}\tilde{\alpha}_{HH}\\ \tilde{\alpha}_{VV}\end{Bmatrix}\right|^2 \qquad (34)$$

The upper line corresponds to σ^0_{VV} and the lower line corresponds to σ^0_{HH}. The Eq. (33) shows explicitly the effect of the non-Gaussian distribution of surface wave slope as well as of the hydrodynamical modulation of short waves, and is easily accessible compared to the integral form given by (24), so that all calculations in the following sections are carried out by using this formula.

3. Azimuth variation of the backscatter cross-section

From (33) we can easily get the difference between the upwind cross-section $\sigma^0{}_u(=\sigma^0|_{\phi=0}$ and the downwind cross-section $\sigma_d{}^0(=\sigma^0|_{\phi=\pi})$

$$\Delta\sigma^0=\sigma_u{}^0-\sigma_d{}^0$$
$$=\frac{1}{2}S_0(k_B)[\{\tilde{T}(1,0;\ \theta,0)-\tilde{T}(-1,0;\ \theta,0)\}$$
$$\times\{Q(1,0)-Q(-1,0)+B(2+Q(1,0)$$
$$+Q(-1,0))\}] \qquad (35)$$

where the following relations have been used,

$$\tilde{T}(\pm1,0;\ \theta,0)=\tilde{T}(\mp1,0;\ \theta,\pi) \qquad (36)$$
$$\tilde{T}(0,\pm1;\ \theta,0)=\tilde{T}(0,\mp1;\ \theta,\pi) \qquad (37)$$
$$Q(\mu,\nu)=Q(\mu,-\nu) \qquad (38)$$
$$S_0(k_B)=\frac{1}{2\pi}S_4(k_B)\left(1+2\frac{1-R}{1+R}\right) \qquad (39)$$

When the distribution of the sea surface slope is Gaussian, we have $Q(\mu,\nu)=0$ so that the difference in backscatter cross-section $\Delta\sigma^0$ is caused only by B in the right-hand side of (35). By substituting (23) and (34) into (35) we get

$$\Delta\sigma^0=S_0(k_B)2\pi k^4\cos^4\theta$$
$$\times\frac{(1+\langle n_1^2\rangle^{1/4}\tan\theta)^4|\tilde{\alpha}_{pp}(1,0;\ \theta,0)|^2}{(1+\langle n_1^2\rangle)^{3/2}}$$
$$\times(1-Z_{pp})(0.04-0.031U+2.06a\sqrt{\langle n_1^2\rangle}) \qquad (40)$$

where

$$Z_{pp}=\left(\frac{1-\sqrt{\langle n_1^2\rangle}\tan\theta}{1+\sqrt{\langle n_1^2\rangle}\tan\theta}\right)^4\frac{|\tilde{\alpha}_{pp}(-1,0;\ \theta,0)|^2}{|\tilde{\alpha}_{pp}(1,0;\ \theta,0)|^2} \qquad (41)$$

and

$$B=a\sqrt{\langle n_1^2\rangle} \qquad (42)$$

Then, Eq. (31) is written as

$$\Delta S(\tilde{\boldsymbol{k}}_B)=an_1S(\boldsymbol{k}_B) \qquad (43)$$

$\tilde{\alpha}_{pp}(\pm1,0)$ is the first-order scattering coefficient refered to a following local incident angle

$$\cos\tilde{\theta}$$
$$=\frac{1}{\sqrt{1+\langle n_1^2\rangle}}\cos\theta[1\pm\sqrt{\langle n_1^2\rangle}\tan\theta] \qquad (44)$$

and could be approximated by (see Appendix)

$$\tilde{\alpha}_{HH}(\pm1,0;\ \theta,0)\fallingdotseq\alpha_{HH}(\theta)\left[1\mp\frac{\sqrt{\langle n_1^2\rangle}}{\sqrt{|\varepsilon|}}\right]^2 \qquad (45)$$

$$\tilde{\alpha}_{VV}(\pm1,0;\ \theta,0)\fallingdotseq\alpha_{VV}(\theta)[1\mp\sqrt{\langle n_1^2\rangle}]^2 \qquad (46)$$

When we introduce (46) into (41), we can see

$$1-Z_{VV}\gtrless0 \quad \theta\gtrless45^0 \qquad (47)$$

However for HH polarization $1-Z_{HH}>0$ for almost all incident angles. In general we can see from (40) that the difference $\Delta\sigma^0$ can be eventually negative for VV polarization, because, in contrast to the coefficient for HH polarization, the local scattering coefficient for VV polarization varies to a large extent according to the variation of the local incident angle $\tilde{\theta}$ of the electromagnetic wave.

It must be noticed that the contribution of the non-Gaussian wave slope distribution in $\Delta\sigma^0$ is in negative sense with respect to the contribution of the hydrodynamical modulation of short gravity-capillary waves. WENTZ (1977: Appendix B) assumed at first that $\Delta\sigma^0$ should be attributed only to the non-Gaussian slope distribution and estimated the coefficients $C_1\sim C_5$ in (23) from observed values of backscatter cross-section. His results gave negative values for C_1 and C_2, which contradicts Cox and Munk's experimental results.

Figure 2(a, b) and Fig 3(a, b) show σ^0 calculated by (33) as well as observed values from the JONSWAP '75 circle flight experiment (MOOR *et al.*, 1978: Appendix A) The dielectric constant

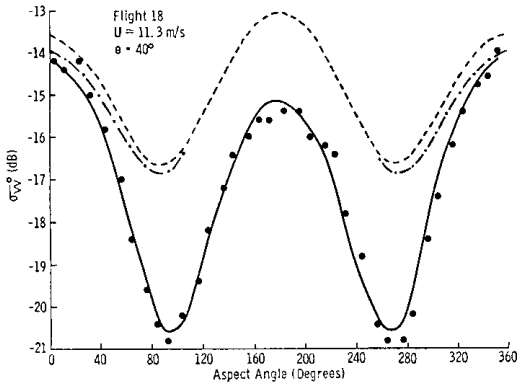

Fig. 2(a). Comparison between theoretical results and observed data on azimuth cross sections variation of backscatter cross sections for *VV*-polalization. The solid line is taken from MOOR *et al.* (1978), the dashed line is for $a=2.5$, and the dash-dot line is for $a=3.5$ in Eq. (43), $\theta=40°$, $U=11.3\ \mathrm{m\,s^{-1}}$.

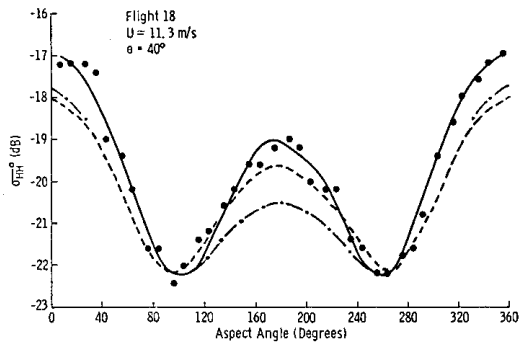

Fig. 2(b). Same as for Fig. 2(a) but for *HH*-polarization.

of sea water used for computation is $\varepsilon=40.1-i39.3$ corresponding to a microwave frequency of 13.9 GHz. The parameter for hydrodynamical modulation a in (43) is assumed to equal 2.5. The general results of the comparison are:

(i) for both *VV* and *HH* polarizations, the difference between upwind and crosswind directions for calculated σ^0 is always smaller than observed. This partly due to the form of the assumed angular spreading factor of the energy spectrum for phigher frequency ocean waves as shown in (5). Originally this form of spectrum comes from a usual Fourier expansion,

$$F(\boldsymbol{k})d\boldsymbol{k}=\frac{1}{\pi}F(k)(1+\sum a_n\cos 2n\phi)kdkd\phi \quad (48)$$

which is only applicable for the case $|\phi|<\pi/2$

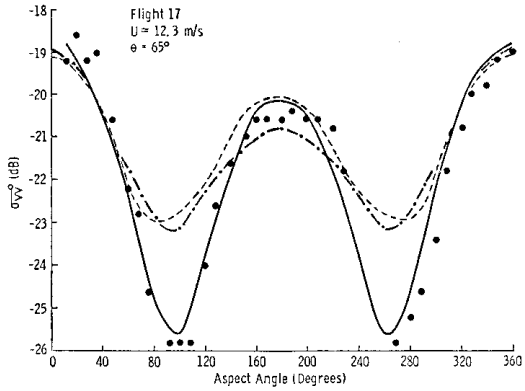

Fig. 3(a). Comparison between theoretical results and data on azimuth variation of backscatter cross sections for *VV*-polarization. The solid line is taken from MOOR *et al.* (1978), the dashed line is for $a=2.5$, and the dash-dot line is for $a=3.5$ in Eq. (43), $\theta=65°$, $U=12.3\ \mathrm{m\,s^{-1}}$.

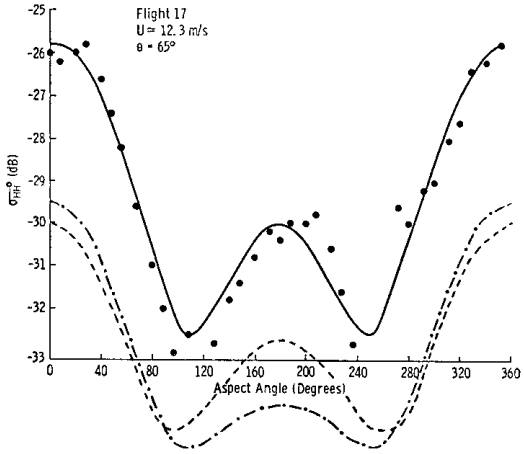

Fig. 3(b). Same as for Fig. 3(a) but for *HH*-polarization.

and $F(\boldsymbol{k})$ vanishes in the other azimuth angles. After simple algebra we get (PIERSON and STACY 1973: eq. (21))

$$a_1=2\frac{1-R}{1+R} \quad (49)$$

As another example, when we assume a cosine-power distribution

$$F(k,\phi)\sim\cos^{2s}\left(\frac{1}{2}\phi\right) \quad (50)$$

we get instead of (5)

$$F(\boldsymbol{k}_B)+F(-\boldsymbol{k}_B)\sim \frac{1}{4\sqrt{\pi}}\frac{\Gamma(s+1)}{\Gamma(s+1/2)} \times\left[\cos^{2s}\left(\frac{\phi}{2}\right)+\sin^{2s}\left(\frac{\phi}{2}\right)\right] \sim \frac{1}{2\pi}\left[1+\frac{s(s-1)}{4+s(s-1)}\cos 2\phi\right] \quad (51)$$

where the following condition is used.

$$\frac{1}{S_4(\boldsymbol{k}_B)}\int_{-\pi}^{\pi} S(\boldsymbol{k}_B)d\phi=1 \quad (52)$$

Actually s is a function of frequency for ordinary ocean waves (LONGUET-HIGGINS 1962), but for short gravity-capillary waves the value of s has not yet been accurately determined. As a tentative value we may take $s=3$ (FUJINAWA, 1980) which gives an angular spreading $(1+0.6\cos 2\phi)$. For $U=12.3\,\mathrm{m\,s^{-1}}$ we get $R=0.685$, which gives a distribution $(1+0.37\cos 2\phi)$, so that by assuming $s=3$ the difference of σ^0 between upwind and crosswind directions increases by about 2.7 dB. This is enough to ameliorate the discrepancy between calculated and observed $\sigma^0_{up}-\sigma^0_{cross}$ in Fig. 2 and Fig. 3. An example of calculations of backscatter cross-section assuming angular spreading of the energy of gravity-capillary waves as expressed in (51) with $s=3$ is shown in Fig. 4.

(ii) For the case $\theta=40$ degrees, contradictory to the observations, calculated σ^0 of VV polarization in the downwind direction is always larger than σ^0 in the upwind direction. On the other hand for the case of $\theta=65$ degrees both polarizations show larger σ^0 in the upwind than in the downwind direction. As we can see from (40) this calculated result depends on the incident angle θ, as well as on both the rather large variations of scattering coefficient due to tilting and/or the wind velocity U in terms of slope variance $\langle n_1^2\rangle$. From a tentative computation of (40) it turns out that for VV polarization $Z_{VV}>1$ for the range $10<u_*<150$ (cm s^{-1}) *i.e.*, σ^0 in the upwind direction is smaller than σ^0 in the downwind direction as long as $\theta<55$ degrees. This result holds even if the step of finite difference decreases to one tenth of the standard deviation, that is $\Delta n_\alpha=0.1\sqrt{\langle n_\alpha^2\rangle}$. On the other hand for HH polarization we get $\sigma^0{}_{\mathrm{up}}>\sigma^0{}_{\mathrm{down}}$ for all incident angles and for arbitrarily friction velocity. For HH polarization $|\tilde{\alpha}_{HH}|<1$ so that the variations of scattering coefficient due to tilting are not so effective as for VV polarization.

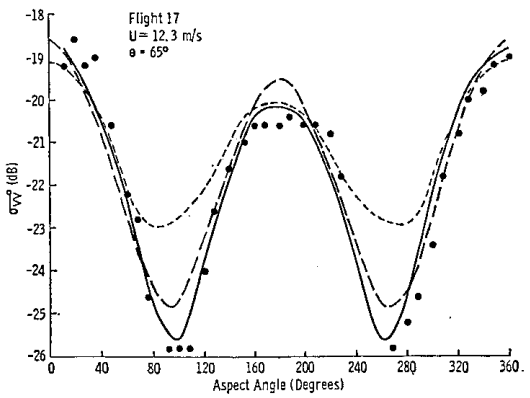

Fig. 4. Same as for Fig. 3(a) but for $a=2.5$. The dotted line is based on angular spreading expressed by Eq. (5) and the dashed line is calculated from Eq. (51) with $s=3$.

As a complementary calculation an expansion of σ^0 in (27) was taken up to the 4th order, but the result for VV polarization shows $\Delta\sigma^0<0$ for the case of $\theta=40$ degrees which corresponds to Fig. 2(a). It must be noticed that the sign of $\Delta\sigma^0$ is independent of the spectrum of ocean waves and is only dependent on the wind velocity, incident angle and scattering coefficient of microwaves.

From consideration of the above we might conclude that the wave-facet model of backscatter represented by (33) can not be applied for $\theta<55$ degrees at least for VV polarization. WENTZ (1978; eq. (16)) postulates on the basis of other reasoning that the facet model should begin to break down at some incident angle θ_b near 40 degrees and proposes that the backscatter due to the Bragg mechanism decreases according to a following purely empirical formula

$$\sigma^0\sim\gamma\tan^2\theta\, e^{-b\tan^2\theta};\ \theta<\theta_b \quad (53)$$

where the coefficients γ and b should be fixed be requiring the value of σ^0 and its first derivative with respect to θ to be continuous at $\theta=\theta_b$.

According to JACKSON (1974: pp. 60-64) there is a fairly continuous transition between specular and Bragg scattering in the neighbourhood of 45 degrees. In the absence of larger waves he puts

$$\sigma^0=W(\theta)\sigma^0{}_{\mathrm{spec}}+[1-W(\theta)]\sigma^0{}_{\mathrm{Bragg}} \quad (54)$$

where the weighting function $W(\theta)$ would be near unity for small angles and fall fairly rapidly to near zero at some critical angle in the neighbourhood of 45 degrees. However the functional form of $W(\theta)$ has not been elucidated.

(iii) For VV polarization the calculated level of backscatter averaged over the azimuth direction is larger than the average observed value and *vice versa* for HH polarization. As discussed above this might be partly due to overestimation of Bragg scattering especially near the transitional incident angle supposed to be 40~45 degrees. However the reasons why the calculated HH polarization for $\theta=65$ degrees is smaller than observed is not clearly understood.

4. Discussion and concluding remarks

Although the wave-facet model fails to reproduce the backscatter cross-section under moderate incident angles, it does give some useful information about nonlinear interactions between short waves and larger waves at least for incident angles larger than 55 degrees. For the case of $\theta=65$ degrees, as shown in Fig. 3(a, b) we get from calculations as well as observations

$$\Delta\sigma^0=\begin{cases} & \text{Cal.} & & \text{Obs.} & \text{Pol.} \\ & a=2.5 & a=3.5 & & \\ & 1.2\,\text{dB} & 1.9\,\text{dB} & 2.0\,\text{dB} & VV \\ & (1.1) & & & \\ & 2.7 & 4.7 & 4.2 & HH \\ & (4.9) & & & \end{cases}$$

where the numerals in parenthesis in the column for $a=2.5$ are obtained when we expand σ^0 in (27) up to the 4th order. In this case we must add in the right-hand side of (27)

$$\frac{1}{4!}\left(\frac{\partial^4\tilde{\sigma}}{\partial\eta_\alpha{}^4}\right)_0\langle n_\alpha{}^4\rangle+\frac{1}{(2!)^2}\left(\frac{\partial^4\tilde{\sigma}}{\partial n_1{}^2\partial n_2{}^2}\right)\langle n_1{}^2n_2{}^2\rangle+\left(\frac{\partial^3\tilde{T}_*}{\partial n_1{}^3}\right)\langle\Delta S n_1{}^3\rangle \qquad (55)$$

where $\alpha=1$ and 2.

From the above we can conclude that 2.5~3.5 is an adequate estimate of α and this gives $B=0.44$~0.62 for $U=10\,\text{m s}^{-1}$. It is interesting to note here that Wentz's model parameters gives $B=0.49$ (HH) and 0.25 (VV).

The modulation of the short-wave spectrum by the larger waves is given in the following form (ALPERS & HASSELMAN, 1978).

$$\frac{\Delta F}{F}=\int R^{\text{hydr}}A(\hat{\boldsymbol{k}})e^{i(\hat{\boldsymbol{k}}\cdot\boldsymbol{x}-\hat{\omega}t)}\,d\hat{\boldsymbol{k}} \qquad (56)$$

where $A(\hat{\boldsymbol{k}})$ represents the Fourier transform of the surface elevation associated with the larger waves, and R^{hydr} denotes modulation transfer function

$$\zeta=\int A(\hat{\boldsymbol{k}})e^{i(\hat{\boldsymbol{k}}\cdot\boldsymbol{x}-\hat{\omega}t)}\,d\hat{\boldsymbol{k}} \qquad (57)$$

Using present notation it can be rewritten as,

$$a=\frac{|R^{\text{hydr}}|}{\hat{k}_x} \qquad (58)$$

where $\hat{k}_x$ denotes wave number of the larger wave in the upwind direction. ALPERS and HASSELMANN (1978) shows by a relaxation model and by choosing Phillips' spectrum $|k_s|^{-4}$ for the short-waves that a increases monotonically from zero and approaches to 4.5

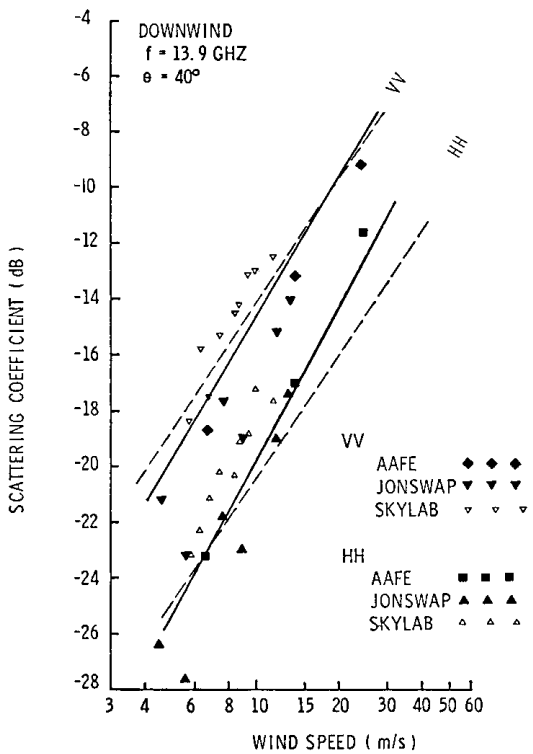

Fig. 5. Comparison of the wind velocity dependence of the backscatter cross-section with observed data. The solid lines are from CHANG & FUNG (1977), and the dashed lines are for $a=2.5$ in eq. (14a).

asymptotically as the ratio of a characteristic relaxation time (μ_*^{-1}) to the period of a characteristic larger wave ($2\pi\omega^{-1}$) exceeds about 1/3.

Based on similar reasoning and by using a relaxation model WRIGHT *et. al.* (1980) estimates $\mu^* \fallingdotseq \beta$ where β is the rate of energy input from the wind and is given by an empirical expression (LARSON and WRIGHT, 1975)

$$\beta = 0.04 \frac{k_s}{c_s} u_*^2 \tag{59}$$

where k_s and c_s are wave number and phase velocity of the short-wave.

For short gravity-capillary waves $\hat{\omega}/\mu_* < 1$ Then, a becomes rather small compared to the above cited values $a = 2.5 \sim 3.5$ (ALPERS and HASSELMAN, 1978: fig. 2). This reasoning suggests that the relaxation time might be longer than previously estimated.

Figure 5 presents the relation of σ^0 to wind velocity for the present model, Chang and Fung's (1973) model, and several observations. The two models agree well with each other except in the case of *HH* at higher wind speed. For higher wind speeds the effect of hydrodynamical modulation becomes predominant especially for *HH* polarization, so that the scattering coefficient $\sigma^0{}_{HH}$ in the downwind direction reduces markedly compared with Chang and Fung's model. We can see from the results that the leading terms of the power series expansion (27) are adequate approximations of the numerical integrals in the badkscatter cross-section problem.

Acknowledgements

The author wishes to thank Mr. T. WATABE of our institute for his help in operating the computer.

Appendix

$$\cos\tilde{\theta}(n_1, 0;\ \theta, 0) = \frac{\cos\theta}{\sqrt{1+n_1{}^2}}(1 + n_1 \tan\theta) \tag{A1}$$

$$\sin\tilde{\theta}(n_1, 0;\ \theta, 0) = \frac{\sin\theta}{\sqrt{1+n_1{}^2}}(1 - n_1 \cot\theta) \tag{A2}$$

We get after simple algebra,

$$[\cos\tilde{\theta} + \sqrt{\varepsilon - \sin^2\tilde{\theta}}]^2 = \frac{1}{1+n_1{}^2} \times [\cos\theta + \sqrt{\varepsilon - \sin^2} + n_1\psi]^2 \tag{A3}$$

where

$$\psi \fallingdotseq \sin\theta - \frac{n_1}{2}\frac{\varepsilon - \cos^2\theta}{\sqrt{\varepsilon - \sin^2\theta}} - \frac{1}{2}\frac{\sin 2\theta}{\sqrt{\varepsilon - \sin^2\theta}} = 0(1) \tag{A4}$$

so that it follows,

$$\tilde{\alpha}_{HH}(\pm 1, 0;\ \theta, 0) \fallingdotseq \alpha_{HH}(\theta) \times \left[1 \mp \frac{\sqrt{\langle n_1{}^2 \rangle}}{\sqrt{|\varepsilon|}}\right]^2 \tag{A5}$$

similarly

$$\tilde{\alpha}_{VV}(\pm 1, 0;\ \theta, 0) \fallingdotseq \alpha_{VV}(\theta)[1 \mp \sqrt{\langle n_1{}^2 \rangle}]^2 \tag{A6}$$

References

ALPERS, W. and K. HASSELMANN (1978): The two-frequency microwave technique for measuring ocean-wave spectra from an airplane or satellite, Boundary-Layer Meteorology, **13**, 215-230.

BARRICK, D. E. and W. H. PEAKE (1967): Scattering from surfaces with different roughness scales: analysis and interpretation. Rep. Battele Memorial Inst. BAT-197A-10-3, 63 pp.

BASS, F. G., I. M. FUKS, A. I. KALMYKOV, I. E. OSTROVSKY and A. D. ROSENBERG (1968a, b): Very high frequency radiowave scattering by a disturbed sea surface, Part 1. IEEE Trans. AP-16, 554-559; Part 2, *ibid*, 650-568.

CHANG, H. L. and A. K. FUNG (1973): Backscattering from a two-scale rough surface with application to radar sea return. NASA Contractor Rep. CR-2327, 63 pp.

CHANG, H. L. and A. K. FUNG (1977): A theory of sea scatter at large incident angles. J. Geophy. Res., **82**, 3439-3444.

COX, C. and W. MUNK (1954): Measurement of the roughness of the sea surface from photographes of the sun glitter. Jour. Opt. Soc. Amer., **44**, 838-850.

FUJINAWA, Y. (1980): Directional spreading of short gravity waves. Rep. Nat'l. Res. Ctr. Disaster prevention (in Japanese), (23), 185-192.

FUNG, A. K. and H. L. CHANG (1969): Backscattering of waves by composite rough surfaces, IEEE Trans., AP-17, 590-597.

HASSELMANN, K. (1971): On the mass and momentum transfer between short gravity waves and large-scale motions. J. Fluid Mech., **50**, 189-205.

JACKSON, F. C. (1974): A curvature-corrected Kirchhoff formulation for radar sea-return from the near vertical. NASA Contractor Rep., CR-2406, 71 pp.

LARSON, T. R. and J. W. WRIGHT (1975): Wind-

generated gravity-capillary waves: laboratory measurements of temporal growth rates using microwave backscatter. J. Fluid Mech., **70**, 417-434.

LONGUET-HIGGINS, M.S. (1962): The directional spectrum of ocean waves and processes of wave generation. Proc. Roy. Soc. London, Ser. A, **265**, 286-315.

MITSUYASU, H. and T. HONDA (1974): The high frequency spectrum of wind generated waves. J. Oceanogr. Soc. Japan, **30**, 29-42.

MOOR, R.K., A.K. FUNG, G.J. DOME and I.J. BIRRER (1978): Estimates of oceanic surface wind speed and direction using orthogonal beam scatterometer measurements and comparison of recent sea scattering theories. NASA Contractor Rep. 158908, 111 pp.

PIERSON, W.J. (1976): The theory and applications of ocean wave measuring systems at and below the sea surface, on the land, from aircraft, and from spacekraft. NASA Contractor Rep. CR-2646, 388 pp.

PIERSON, W.J. and R.A. STACY (1973): The elevation, slope, and curvature spectra of a wind roughned sea surface. NASA Contractor Rep. CR-2247, 126 pp.

RICE, S.O. (1951): Reflection of electromagnetic waves from slightly rough surfaces. Cmm. Pure Appl. Math., **4**, 351-378.

VALENZUELLA, G.R. (1968): Scattering of electromagnetic waves from a tilted slightly rough surface. Radio Sci., **3**, 1057-1066.

WENTZ, F.J. (1977): A two-scale scattering model with application to the JONSWAP '75 aircraft microwave scatterometer experiment. NASA Contractor Rep. 2919, 122 pp.

WENTZ, F.J. (1978): Estimation of the sea surface's two-scale backscatter parameters. NASA Contractor Rep. 145255, 122 pp.

WRIGHT, W.J. (1966): Backscattering from capillary waves with application to sea clutter. IEEE Trans. AP-14, 740-754.

WRIGHT, W.J., W.J. PLANT, W.C. KELLER and W.L. JONES (1980): Ocean wave-radar modulation transfer functions from the West Coast Experiment. J. Geophy. Res., **85**, 4957-4966.

海面からのマイクロ波後方散乱と短周期重力波スペクトルの変調

岩　田　憲　幸*

要旨: いわゆる wave-facet モデルによって海面からのマイクロ波後方散乱断面積を求め JONSWAP (1975 年) の実験結果と比較した．主な結果は (1) 風上方向と風下方向の後方散乱断面積の差違は長い波による短周期波の変調によるもので，波面勾配分布がガウス過程からずれる効果とは相殺するように働く．(2) 高周波波浪の方向スペクトル幅は cosine 分布より狭くなる．(3) wave-facet モデルそれ自身の適用限界の下限を示すマイクロ波の入射角は今迄考えられていたものより大きい．

* 国立防災科学技術センター平塚支所
〒254 神奈川県平塚市虹ケ浜9-2